Interfacial-Redox-Induced Tuning of Superconductivity in $YBa_2Cu_3O_{7-\delta}$

Peyton Murray[1], Dustin Gilbert[2], Alexander J. Grutter[2], Brian J. Kirby[2], David Hernandez-Maldonado[3], Maria Varela[3], Zachary E. Brubaker[1,4], Rajesh V. Chopdekar[5,6], Valentin Taufour[1], Rena Zieve[1], Jason R. Jeffries[4], Elke Arenholz[6], Yayoi Takamura[5], Julie Borchers[2], Kai Liu[1,7]

[1]*Physics Department, University of California, Davis, CA 95616*

[2]*NIST Center for Neutron Research, National Institute of Standards and Technology, Gaithersburg, MD 20899*

[3]*Universidad Complutense de Madrid, Madrid 28040, Spain*

[4]*Lawerence Livermore National Laboratory, Livermore, CA 94550*

[5]*Department of Materials Science and Engineering, University of California, Davis, CA 95616*

[6]*Advanced Light Source, Lawrence Berkeley National Laboratory, Berkeley, CA 94720*

[7]*Physics Department, Georgetown University, Washington, DC 20057*

Many of the properties of the high-T_c copper oxide superconductors are strongly influenced by charge doping[1,2]. The ability to control the doping level in these materials is therefore important not only for the development of experimental platforms that enable studies of correlated electron physics, but for multifunctional device applications as well. While traditionally[3–6] the doping level is fixed during synthesis via chemical substitution or post-growth annealing, recently several techniques have demonstrated approaches which allow for on-demand control. By leveraging electrolytic double layer techniques, gating experiments[7,8] on $RBa_2Cu_3O_{7-\delta}$ (R=Y, Nd) thin films have achieved control over the Cu-site doping level, which determines the dominant electronic order, by introducing oxygen vacancies into the film under electric fields. In these materials, O^{2-} ions can migrate under the influence of an externally applied electric field to eventually escape through the film surface, resulting in the formation of oxygen vacancies. To maintain charge neutrality electrons are returned to the Cu ions within the film, resulting in a reduction in Cu valence and reducing the hole concentration of the oxide. Signatures of the effects on the electronic order in these materials are profound, and point to the effectiveness of oxygen migration and vacancy formation in manipulating the properties of the cuprate superconductors. Recently, we demonstrated a different, solid-state approach to manipulate ionic distributions in oxide thin films by using a reactive Gd capping layer and thus achieve ionic control of magnetism.[9–11] Leveraging the reactivity of Gd, these capping layers can extract oxygen from an adjacent oxide film, with the level of oxygen depletion controlled by the thickness of the Gd and the ion mobility in the oxide, often at room-temperature. Superconducting $YBa_2Cu_3O_{7-\delta}$ (YBCO) is a prototypical example of the high-T_c cuprates, with crystal structure and electronic ordering sensitive to oxygen stoichiometry. Combined with its high ionic conductivity,[12,13] these properties make it an ideal candidate material to explore with this method.

In this study Gd capping layers of varying thicknesses are deposited on 100 nm thick $YBa_2Cu_3O_{7-\delta}$ films, dramatically altering the oxygen distribution throughout the underlying film without any annealing. As the Gd layer thickness (t_{Gd}) is increased the YBCO layer becomes progressively more oxygen deficient, demonstrating how appropriate tuning of t_{Gd} can precisely control the remaining

oxygen content of the underlayer. The extraction of oxygen from the YBCO induces a structural transition and alters the superconductivity by reducing and broadening the superconducting transition temperature. Superconductivity is completely extinguished for the sample with thickest capping layer. X-ray absorption spectra (XAS) indicate a reduction of Cu valence state consistent with the removal of oxygen from the YBCO film, particularly from within the CuO chains. Since superconductivity in YBCO relies on charge transfer from the CuO chains to the CuO_2 planes, the disappearance of superconductivity may be attributable to the reduction in hole doping level or structural changes, both effects induced by Gd-driven oxygen migration.

Films of $YBa_2Cu_3O_{7-\delta}$ (100 nm) were grown on (001) $SrTiO_3$ (STO) substrates using pulsed laser deposition[14]. The high-symmetry STO substrate (cubic, lattice parameter of 3.905 Å) is expected to grow with a degenerate epitaxy, forming 90° twinned domains[15], with up-to 2% tensile strain exerted at the interface due to lattice mismatch[16,17] (bulk lattice parameters of YBCO are exptected to be a = 3.827 Å, b = 3.893 Å, and c = 11.699 Å[18]). While the strain is known to suppress T_C, the films are expected to relax away from the substrate/film interface[19,20] and show near bulk-like superconducting behavior[17]. The films were then sputter coated with Gd layers of varying thickness (t_{Gd} = 3 nm, 7 nm, 20 nm) and an Au (5 nm) protective cap, with one film kept in the as-grown state for comparison. X-ray diffraction (XRD) scans of the as-grown film, measured along the out-of-plane direction (Fig. 1a) show only the $(00l)$ family of peaks and give a c-axis lattice parameter of 11.678 Å, similar to the bulk values[18]. The slightly smaller c-axis lattice parameter may be due to the tensile strain from the substrate[21]. As t_{Gd} is increased, a monotonic shift towards lower 2θ is observed in the YBCO $(00l)$ diffraction peaks indicating expansion in the c-axis. Similar lattice expansion has previously been noted in other perovskite systems[22] and is a signature of oxygen depletion. In addition to the out-of-plane direction, the in-plane structure of the films was probed using reciprocal space maps (RSMs) taken near the $(\acute{1}03)$ STO substrate reflection (Fig. 1b-e, g-j). Coordinate axes of the RSMs identify the h (x-axis) and l (y-axis) Miller indices relative to the STO substrate. When grown on cubic STO substrate, nominally orthorhombic YBCO is expected to form

a twinned crystal structure, resulting in a splitting of the in-plane Bragg reflections[16]. The RSMs show a bright substrate peak near the top of each map, with a lower-intensity YBCO peak near $h = -1.01, l = 2.67$, elongated in the in-plane direction, and consistent with the presence of two overlapping Bragg reflections from $(\bar{1}08)$ and $(0\bar{1}8)$ YBCO crystal planes. Importantly, the spread of the YBCO film peak along the $(h00)$ direction, even in the as-grown sample, indicates the films were relaxed in-plane and possess the expected orthorhombic distortion before the Gd capping layers were deposited. As t_{Gd} is increased, the film peak broadens along the (00l) direction and shifts to lower l, consistent with an expansion in the *c*-axis lattice parameter as seen in the symmetric $\theta - 2\theta$ scans discussed above. In addition to simple lattice expansion with increasing t_{Gd}, a second broader feature emerges at lower angles alongside the $(00l)$ peaks, particularly visible in the $\theta - 2\theta$ scans, associated with the optimally doped phase (OP) for $t_{Gd} = 7$ nm. This secondary, oxygen-deficient (OD) phase becomes dominant for $t_{Gd} = 20$ nm.

The Gd capping layer is expected to extract oxygen from the YBCO, resulting in structural changes observed in XRD patterns. Cross-sectional high-angle annular dark field scanning transmission electron microscopy (HAADF-STEM) images of the as-grown film at the STO/YBCO interface show flat, epitaxial YBCO growth consistent with XRD patterns. The layered structure of $YBa_2Cu_3O_{7-\delta}$ is well resolved, with bright Ba-Y-Ba atoms visible between alternating horizontal rows of dark CuO chains, and occasional double-CuO layer stacking faults distributed throughout (Fig. 2a). Examples of double-CuO stacking faults have been reported in YBCO previously, particularly in PLD grown films[23]. In the $t_{Gd} = 3$ nm and 7 nm Gd-capped samples, double-CuO stacking faults appear near the surface of the film, with major lattice distortions visible in the $t_{Gd} = 20$ nm film (Fig. 2b-d). These defects point to the interfacial nature of the oxygen leaching effect, as the YBCO layers nearest the Gd interface become increasingly disrupted when oxygen is removed from deep within the film.

The extraction of oxygen was further probed by polarized neutron reflectometry (PNR), which provides a depth-resolved mapping of the nuclear scattering centers within the film. The converged depth

profiles (Fig. 3) confirm the expected 100 nm thickness of the as-grown structure, while the nuclear scattering length density (SLD, ρ_N) of the as-grown film is similar to the calculated value for $YBa_2Cu_3O_7$ of $4.7 \times 10^{-4} nm^{-2}$. With increasing t_{Gd} the YBCO layer increases in thickness, in agreement with the unit cell expansion observed in XRD. Commensurate with the progressive increase in thickness, the nuclear SLD decreases, particularly near the YBCO/Gd interface. The decrease of ρ_N is consistent with the removal of oxygen from the YBCO. In addition to the standard nuclear profile, the Gd layer is explicitly identifiable by the imaginary component of its SLD, which corresponds with neutron absorption. The imaginary component of the Gd SLD allows us to rule out the possibility of YBCO/Gd interdiffusion.

While the PNR results are consistent with the extraction of oxygen from the YBCO, fluorescence yield (FY) XAS measurements performed at the Cu $L_{2,3}$-edges directly confirm a change in the Cu valence resultant from the oxygen extraction. The XA results (Fig. 4) show a shift in the absorption resonance to lower energies with increasing t_{Gd}.. Similar spectral shifts reported in other oxygen-deficient perovskite systems[24,25] have been attributed to a decrease in the average Cu valence, the result of electrons returning to the Cu ions as oxygen is leached from the film. The shoulder at 933.5 eV in the as-grown YBCO spectra, a feature characteristic of lower-valence ligand states present in CuO chains[8,26–28], is suppressed for greater t_{Gd}, confirming the loss of oxygen within the chains. A second resonance associated with the Cu^{1+} valence state emerges at 934 eV for $t_{Gd} = 7$ nm and 20 nm. This new absorption peak, appearing in conjunction with the emergent low angle feature observed in XRD, again points to the formation of a stable OD phase. The bulk sensitivity of FY measurements (70% X-ray transmission through 100 nm of YBCO at Cu-L_2 resonance) infers that the observed oxygen depletion comes from ionic migration from deep within the film despite the interfacial origin of the leaching effect. The high ionic conductivity required for such long-range oxygen migration is in agreement with previous reports.[12,13] The known sensitivity of the YBCO superconductivity to the oxygen stoichiometry suggests that this approach may therefore be used as a mechanism to design the superconducting transition.

To examine the effects of Gd deposition on the YBCO superconducting properties, magnetometry and Van der Paw resistivity measurements were performed between 5 K - 100 K. Zero-field cooled (ZFC) measurements of the magnetic moment (Fig. 5a, b) show a sharp phase transition in the as-grown YBCO film at $T_c \approx 84$K, typical of YBCO films grown on STO substrates[17], indicating rejection of the magnetic field due to the Meissner effect, and indicating the superconducting transition. Accompanying the magnetic transition is a precipitous drop in resistivity, further confirming the superconducting transition. With increasing Gd capping layer thickness the magnetic transition shows a smooth reduction in the transition temperature T_c, with complete suppression of the Meissner effect for $t_{Gd} = 20$ nm. In contrast to the magnetometry, resistivity measurements initially show only a small shift toward lower T_c for $t_{Gd} = 3$ nm. However, for $t_{Gd} = 7$ nm and 20 nm the superconducting transition is completely suppressed, with no apparent transition down to the lowest measured temperature (5 K).

The differences between the superconducting transitions observed in magnetometry and resistivity can be explained by the presence of a low-T_c, high-resistivity OD phase stabilized alongside the OP phase YBCO film. Specifically, for the as-prepared and $t_{Gd} = 3$ nm samples, a majority of the film possesses the initial structure and nominal stoichiometry of $YBa_2Cu_3O_{7-\delta}$ where $0 < \delta < 0.5$. By comparison, the $t_{Gd} = 7$ nm sample shows a transition in the magnetometry, but not in the resistivity. The magnetic signal arises from the Meissner effect and will scale directly with the superconducting volume fraction of the film, while the superconducting transition in the resistivity necessitates a continuous superconducting pathway to exist through the sample. Therefore, the $t_{Gd} = 7$ nm sample possesses some fraction which is still superconducting, as evidenced by the magnetometry, but is beyond the percolation limit for the resistive OD phase, as evidenced by the absence of a transition in the resistance. Finally, for the thickest $t_{Gd} = 20$ nm sample the absence of a transition in either the resistance or magnetic data suggests few, if any, domains remain which undergo a superconducting transition. The distinctly different superconducting properties of the OD phase may be the result of structural changes - including ordering or strain - or electron doping, both of which are consequences of the oxygen leaching.

In summary, Gd capping layers deposited at room temperature on optimally doped YBCO thin films have been shown to remove oxygen from the underlying film via an interfacial redox reaction, with the amount removed dependent on capping layer thickness. The superconducting transition temperature is significantly reduced, and for sufficient thickness of Gd is extinguished completely. X-ray spectroscopy measurements indicate the CuO planes become progressively more oxygen deficient with increasing Gd thickness, while the emergence of a separate peak in XRD indicates the formation of a separate structural phase, suggesting that both structural changes as well as a reduction in hole doping level may play roles in the suppression of superconductivity. Remarkably, the changes to the superconducting properties throughout the entire 100 nm thick YBCO films are induced by the migration of oxygen towards the YBCO/Gd interface, extending the viability of this approach for controlling the hole-doping level to the quasi-bulk regime.

Supplementary Information

Experimental Methods. Commercially available 100 nm thick YBCO films grown on STO substrates were purchased and subsequently sputter coated with Gd (3 nm, 7 nm, 20 nm) and a Au (5 nm) protective capping layer using Ar gas at 0.67 Pa working pressure in a chamber with a base pressure of 1×10^{-5} Pa. XRD characterization, including both $\theta - 2\theta$ symmetric scans and reciprocal space maps, was performed on a X-ray diffractometer equipped with parallel beam optics and Cu $K\alpha_1$ monochromator. Polarized neutron reflectometry was measured at the NIST Center for Neutron Research on the PBR and MAGIK beamlines. The experiment used 5 Å neutrons, and were carried out at a temperature of 6 K. Fitting of the PNR data was performed using the Refl1d software package, following a Markov-chain Monte Carlo fitting algorithm[29]. The calculated SLD was determined by the calculating the sum of the volume-scaled atomic scattering lengths. XA measurements were performed at the Advanced Light Source on beamline 4.0.2 at room temperature in a grazing incidence (30°) geometry. Both fluorescence and electron yield (EY) modes were measured, but due to the capping layers no appreciable signal was measured in the EY mode. Magnetometry measurements, FC and ZFC, were performed in a field of 1 mT. To reduce stray magnetic fields, the magnet was purged before each measurement. Resistivity was measured using a four-contact Van der Pauw geometry. The current used was $100\mu A$ at frequency of 173 Hz. The magnetic field at the sample was set to zero before the measurement by setting the temperature to the midpoint of the superconducting transition before adjusting the applied field to minimize the resistivity.

References

1. Cava, R. J. *et al.* Structural anomalies at the disappearance of superconductivity in $Ba_2YCu_3O_{7-\delta}$: Evidence for charge transfer from chains to planes. *Phys. C Supercond.* **156,** 523–527 (1988).

2. Blanco-Canosa, S. *et al.* Resonant X-ray Scattering Study of Charge Density Wave Correlations in $YBa_2Cu_3O_{6+x}$. *Phys. Rev. B* **90,** 054513 (2014).

3. Presland, M. R., Tallon, J. L., Buckley, R. G., Liu, R. S. & Flower, N. E. General trends in oxygen stoichiometry effects on Tc in Bi and Tl superconductors. *Phys. C Supercond. its Appl.* **176,** 95–105 (1991).

4. Lee, P. A., Nagaosa, N. & Wen, X. G. Doping a Mott insulator: Physics of high-temperature superconductivity. *Rev. Mod. Phys.* **78,** (2006).

5. Groen, W. A., de Leeuw, D. M. & Geelen, G. P. J. Hole concentration and Tc in $Bi_2Sr_2CuO_{6+\delta}$. *Phys. C Supercond. its Appl.* **165,** 305–307 (1990).

6. Humphreys, R. G. *et al.* Physical vapour deposition techniques for the growth of $YBa_2Cu_3O_7$ thin films. *Supercond. Sci. Technol.* **3,** 38–52 (1990).

7. Perez-Muñoz, A. M. *et al.* In operando evidence of deoxygenation in ionic liquid gating of $YBa_2Cu_3O_{7-X}$. *Proc. Natl. Acad. Sci.* **114,** 215–220 (2017).

8. Zhang, L. *et al.* The Mechanism of Electrolyte Gating on High-Tc Cuprates: The Role of Oxygen Migration and Electrostatics. *ACS Nano* **11,** 9950–9956 (2017).

9. Gilbert, D. A. *et al.* Controllable positive exchange bias via redox-driven oxygen migration. *Nat. Commun.* **7,** 11050 (2016).

10. Grutter, A. J. *et al.* Reversible control of magnetism in $La_{0.67}Sr_{0.33}MnO_3$ through chemically-induced oxygen migration. *Appl. Phys. Lett.* **108,** 082405 (2016).

11. Gilbert, D. A. *et al.* Structural and magnetic depth profiles of magneto-ionic heterostructures beyond the interface limit. *Nat. Commun.* **7,** 12264 (2016).

12. Shen, G. J., Lam, C. C., Chow, J. C. L. & Tang, S. T. Twin formation due to irradiation of energetic electron beam in high-temperature superconductors of In- and Sb-doped YBCO. *Phys. C Supercond. its Appl.* **214,** 426–434 (1993).

13. Muller, J. H., Mertin, W. & Gruehn, R. Oxygen mobility in $YBa_2Cu_3O_{7-x}$: A TEM and HRTEM investigation. *Supercond. Sci. Technol.* **3,** 273–281 (1990).

14. Lorenz, M. *et al.* High-quality Y-Ba-Cu-O thin films by PLD-ready for market applications. *IEEE Trans. Appiled Supercond.* **11,** 3209–3212 (2001).

15. Phillips, J. M. Substrate selection for high-temperature superconducting thin films. *J. Appl. Phys.* **79,** 1829–1848 (1996).

16. Budai, J. D., Feenstra, R. & Boatner, L. A. X-ray study of in-plane epitaxy of $YBa_2Cu_3O_x$ thin films. *Phys. Rev. B* **39,** 12355–12358 (1989).

17. Zhai, H. Y. & Chu, W. K. Effect of interfacial strain on critical temperature of $YBa_2Cu_3O_{7-\delta}$ thin films. *Appl. Phys. Lett.* **76,** 3469–3471 (2000).

18. Calestani, G. & Rizzoli, C. Crystal structure of the $YBa_2Cu_3O_7$ superconductor by single-crystal X-ray diffraction. *Nature* **328,** 606–607 (1987).

19. Lin, W. J., Hatton, P. D., Baudenbacher, F. & Santiso, J. Observation of small interfacial strains in $YBa_2Cu_3O_x$ sub-micron-thick films grown on $SrTiO_3$ substrates. *Appl. Phys. Lett.* **72,** 2966–2968 (1998).

20. Granozio, F. M., Ricci, F., Scotti di Uccio, U. & Villegier, J. C. Orthorhombic-tetragonal transition in twin-

free (110) YBa2Cu3O7 films. *Phys. Rev. B* **57,** 6–9 (1998).

21. Xie, C., Budnick, J. I., Wells, B. O. & Woicik, J. C. Separation of the strain and finite size effect on the ferromagnetic properties of $La_{0.5}Sr_{0.5}CoO_3$ thin films. *Appl. Phys. Lett.* **91,** 172509 (2007).

22. Miyoshi, S. *et al.* Lattice expansion upon reduction of perovskite-type $LaMnO_3$ with oxygen-deficit nonstoichiometry. *Solid State Ionics* **161,** 209–217 (2003).

23. Ramesh, R. *et al.* Direct Observation of Structural Defects in Laser-Deposited Superconducting Y-Ba-Cu-O Thin-Films. *Science* **247,** 57–59 (1990).

24. Li, B. *et al.* Tuning interfacial exchange interactions via electronic reconstruction in transition-metal oxide heterostructures. *Appl. Phys. Lett.* **109,** 152401 (2016).

25. Lu, N. *et al.* Electric-field control of tri-state phase transformation with a selective dual-ion switch. *Nature* **546,** 124–128 (2017).

26. Chen, C. T. *et al.* Out-of-plane orbital characters of intrinsic and doped holes in $La_{2-x}Sr_xCuO_4$. *Phys. Rev. Lett.* **68,** 2543–2546 (1992).

27. Nücker, N. *et al.* Site-specific and doping-dependent electronic structure of YBa2Cu3Ox probed by O 1*s* and Cu 2*p* x-ray-absorption spectroscopy. *Phys. Rev. B* **51,** 8529–8542 (1995).

28. Bianconi, A. *et al.* Localization of Cu 3d levels in the high Tc superconductor $YBa_2Cu_3O_{\sim 7}$ by Cu 2*p* X-ray photoelectron spectroscopy. *Solid State Commun.* **63,** 1135–1139 (1987).

29. Kirby, B. J. *et al.* Phase-sensitive specular neutron reflectometry for imaging the nanometer scale composition depth profile of thin-film materials. *Curr. Opin. Colloid Interface Sci.* **17,** 44–53 (2012).

Figures

Figure 1. XRD $\theta - 2\theta$ scan (a) near the (002) YBCO peak measured with Cu $K\alpha_1$ radiation. Reciprocal space maps (b-e) showing the $(\acute{1}03$ STO substrate peak at top, with $(\acute{1}08)/(0\acute{1}8)$ YBCO peak at bottom (g-j), and projections (f, k) of each map along the l-direction.

Figure 2. Cross-sectional HAADF-STEM images of the as-grown STO/YBCO interface (a), the YBCO/Gd interfaces of the Gd (3 nm) (b) and Gd (7 nm) (c) samples, and center of the Gd (20 nm) film (d).

Figure 3. Real (a) and imaginary (b) part of the nuclear SLDs as a function of depth z through the sample as measured by PNR. Grey region ($z < 0$) corresponds to the substrate, with the approximate location of the YBCO, Gd, and Au layers given by the shaded regions for ($z > 0$).

Figure 4. Close-up view of the normalized absorption spectra as a function of incident X-ray photon energy near the Cu L_3-edge, as measured in fluorescence yield mode. The full spectral range measured including the Cu L_2-edge is shown in the inset, with the shaded region corresponding to the close-up view.

Figure 4. Normalized magnetization (a) and resistivity (b) as functions of temperature. The Gd (20 nm) sample has been omitted from (b), as no magnetic moment was detected at any temperature measured (to within experimental noise).

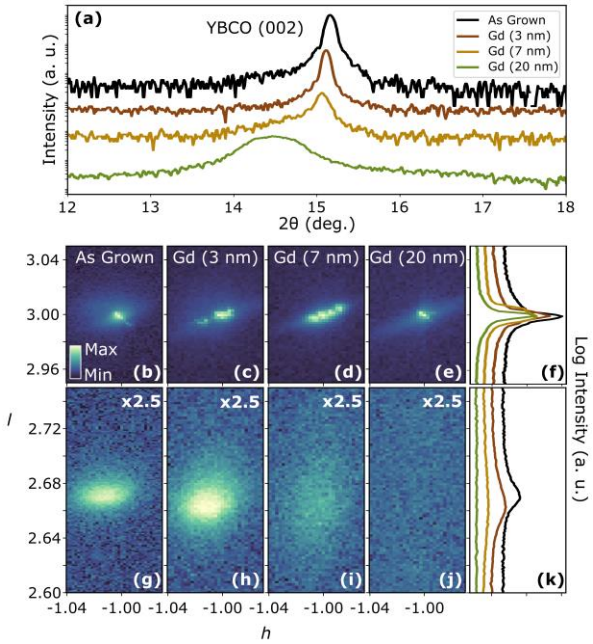
(a)
YBCO (002)
As Grown
Gd (3 nm)
Gd (7 nm)
Gd (20 nm)
Intensity (a. u.)
2θ (deg.)
Max
Min
(b)
(c)
(d)
(e)
(f)
(g)
(h)
(i)
(j)
(k)
x2.5
Log Intensity (a. u.)
l
h

Figure 1

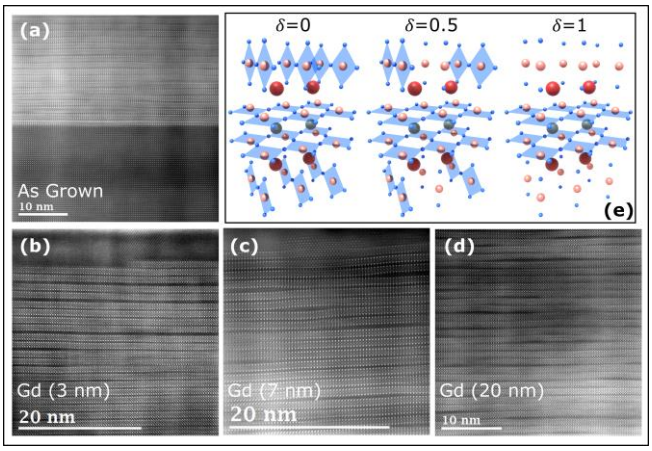
(a)
As Grown
10 nm
δ=0
δ=0.5
δ=1
(e)
(b)
Gd (3 nm)
20 nm
(c)
Gd (7 nm)
20 nm
(d)
Gd (20 nm)
10 nm

Figure 2

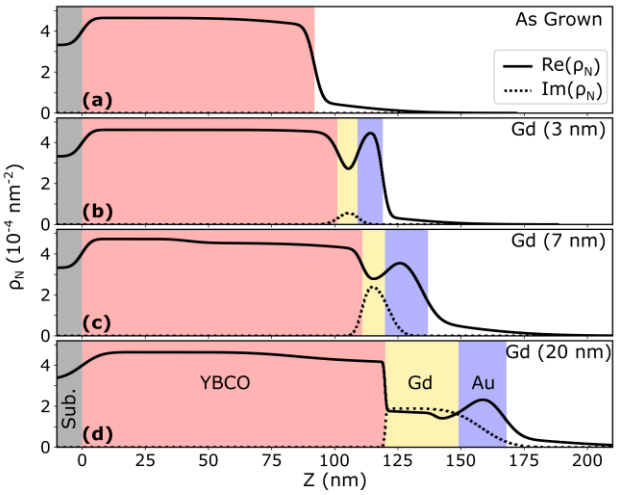
As Grown
Re(ρN)
Im(ρN)
(a)
Gd (3 nm)
(b)
Gd (7 nm)
(c)
Gd (20 nm)
Sub.
YBCO
Gd
Au
(d)
ρN (10-4 nm-2)
Z (nm)
0
25
50
75
100
125
150
175
200
0
2
4

Figure 3

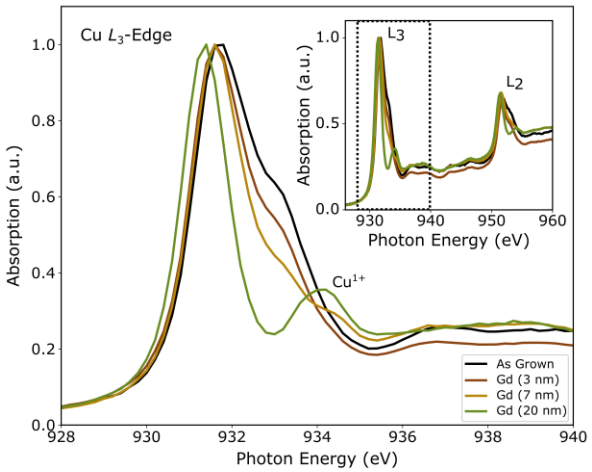
Cu L_3-Edge
Absorption (a.u.)
Photon Energy (eV)
L_3
L_2
Cu^{1+}
As Grown
Gd (3 nm)
Gd (7 nm)
Gd (20 nm)

Figure 4

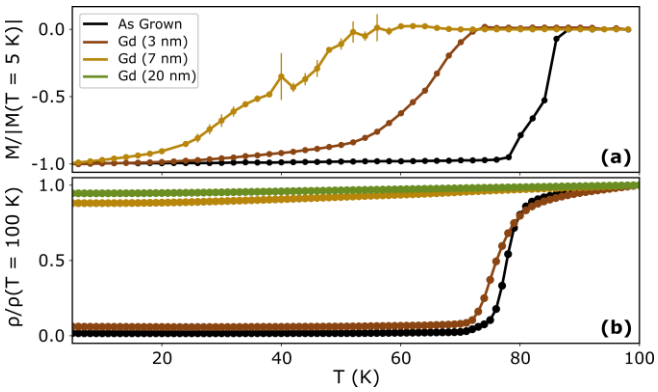
As Grown
Gd (3 nm)
Gd (7 nm)
Gd (20 nm)
M/|M(T = 5 K)|
0.0
-0.5
-1.0
(a)
ρ/ρ(T = 100 K)
1.0
0.5
0.0
(b)
20
40
60
80
100
T (K)

Figure 5